Microembossed copper microchannel heat sink for high-density cooling in electronics

Xuanyang Li, Jing Chen ✉

Institute of Microelectronics, Peking University, Beijing 100871, People's Republic of China
✉ *E-mail: j.chen@pku.edu.cn*

Published in Micro & Nano Letters; Received on 10th April 2019; Revised on 12th July 2019; Accepted on 15th August 2019

A microembossed copper microchannel heat sink was designed and fabricated for high-density cooling in electronics. The microchannel width and aspect ratio were investigated to find out the optimised channel size for microembossing. The fabrication method was based on bulk copper forming including tungsten die inductively coupled plasma etching, hot copper microembossing, inlet/outlet ports punching and sealing. The heat dissipation performances were tested by ceramic heater. The maximum temperature decreased to ~37°C under different heat fluxes, with the maximum temperature decreased by 69.2% at 50 W/cm^2 heat flux. The equivalent heat transfer coefficient reached the value of 6492 W/m^2 K. High-power chip was used as heat source too. The maximum heat flux reached 304.8 W/cm^2 when the chip can still function properly at 90.5°C. High cooling performance with the micro-heat sink proves that microembossing by tungsten die is an alternative process for microchannel heat sink fabrication with batch production and low cost. Taking advantages of simple fabrication process and reutilisation of tungsten die, the technology shows promising potentials in high-density microcooling systems.

1. Introduction: With the development of very large-scale integrating technology, minimisation and high integration of microelectronic devices have led to significant increase of power densities. The electrical performances are strongly affected by operating temperature. Nearly, 60% of electronic failures are caused by high temperature, and for every 10°C temperature rising, the failure rate nearly doubles [1]. With the concentration of chips heat generation, the traditional forced air convection cooling method is not sufficient for next-generation high-power chips; thus, microcooling technologies with high efficiency are urgently needed to ensure the proper functioning of the microchips [2].

The first study of microchannel heat sink for microcooling was raised by Tuckerman and Pease [3]. The 10mm × 10 mm silicon microchannel heat sink shows a maximum thermal resistance of 0.09 cm^2 K/W, at a heat flux of 790 W/cm^2 for a flow rate of 0.61 l/min and a pressure drop of 2 bar. After that, various researches on microchannel heat sink have been studied both numerically and experimentally including pin fin geometry [4–6], inlet/outlet layout [7, 8] and multi-layer structures [9–11]. Except for the microstructure and micro-heat sink layout, flow boiling [12, 13] and nanofluids cooling [14, 15] were also found related to improving heat transfer capability. Owing to the mature technology in semiconductor fabrications, these microcooling researches were mainly applied on silicon substrate microchannels. However, compared to metal materials such as copper and aluminium (Al), silicon has disadvantages in heat conduction, which limits the higher cooling efficiency.

Several types of researches on Al and copper micro-heat sink have been studied. Microfabrication method for metal materials was developed for micrometre scale. In the previous researches, different microfabrication methods are applied such as ultraviolet-Lithographie, Galvanoformung, Abformung (LIGA) technology [16, 17], micromilling [18–20] and wire-cut electro-discharge machining [21, 22]. All of the micro-heat sinks show good cooling capability. However, due to the complicated fabrication process and high cost, there is still a long distance to mass production. Simple fabrication technology, which is more suitable for high-power applications, needs to be further developed.

This Letter presents a novel bulk copper microembossing method for the microchannel heat sink, which is less complicated and low cost. Tungsten was used as a die material in hot copper microembossing. The whole fabrication process contains tungsten inductively coupled plasma (ICP) etching, copper microembossing, inlet/outlet port punching and top/bottom plates sealing. Microchannel parameters including channel width and aspect ratio were analysed in consideration of the cooling performance and fabrication capability. Cooling tests were raised using both ceramic heater and high-power chip. The experimental results show that this technology is an alternative process for micro-heat sink fabrication with mass production.

2. Design and analysis: The micro-heat sinks are expected to be integrated with packaging box for chip cooling on printed circuit board (PCB) board, as shown in Fig. 1*a*. The whole cooling systems consist of multi-layer board (including PCB board and packaging box) and liquid pipes on vertical directions. Microchannel heat sinks are placed under the PCB board, assembling in specially made metal packaging box with microchannel connections. The coolant flows from the inlet pipe to the packaging box and microchannel heat sink to take away heat flux on the chips.

A typical microchannel arrangement is chosen, as shown in Fig. 1*b*. Microchannels are designed both on the top plate and bottom plate. Inlet/outlet ports are placed on the bottom, and guide channels near the inlet/outlet ports are applied to distribute the liquid flow to each single microchannels.

To figure out the optimised dimension of microchannels, simulations of micro-heat sink model were performed by COMSOL 5.2. The governing equations are continuity (1), momentum conservation (2) and energy conservation (3)

$$\nabla \cdot (\rho u) = 0 \tag{1}$$

$$\rho \cdot (\boldsymbol{u} \cdot \nabla u) = F - \nabla p + \mu \nabla^2 u \tag{2}$$

$$\rho c_{\mathrm{p}} \cdot (\boldsymbol{u} \cdot \nabla T) = k \nabla^2 T + \Phi \tag{3}$$

In the above equations, ρ is the density of the coolant, u is the velocity and T is the temperature while p is the pressure and μ is the dynamic viscosity. c_{p} is the specific heat and k is the thermal conductivity. Φ is the heat intensity and F is the driving force. Both of them are zero in this case.

In the simulation, the heater was chosen as pure aluminium oxide ceramic. The heat source was set as 40 W/cm^2 on the top surface, and the inlet flow rate was 10 ml/min. Deionised water was used

doi: 10.1049/mnl.2019.0198

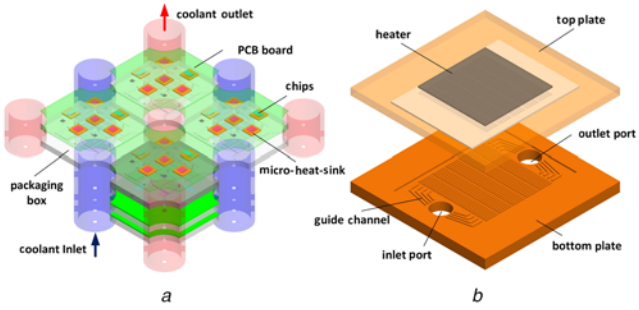

Fig. 1 *Designation and application of micro-heat sink*
a Schematic diagram of micro-heat sinks for chip cooling on PCB board
b Designation of a typical single-phase micro-heat sink

as coolant, and the flow regime was set as incompressible and continuous.

The channel width and aspect ratio are important factors of both heat removal and pressure drop. As microembossing height and channel width are limited by microfabrication capability, it is important to find out the optimised parameters. First, the influence of the channel width was investigated. Microchannels with different channel widths from 30 to 150 µm were applied, while the space ratio of microchannel is 1.2 and the aspect ratio is 1. The minimum temperature occurs near the inlet port, and the maximum temperature occurs near the outlet port. The maximum temperature and pressure drop between inlet/outlet are extracted from the simulation results, as shown in Fig. 2*a*. The maximum temperature on the chip shows almost no differences when the channel width increases from 30 to 150 µm, which is mainly due to the same proportion between solid and fluid. However, there is an obvious increase in pressure drop when the channel width decreases below 80 µm. The larger pressure drop requires a higher sealing strength of micro-heat sink.

The influences of aspect ratio were investigated too, as shown in Fig. 2*b*. The maximum temperature shows a significant decrease with increasing aspect ratio. This phenomenon is obvious because of the increasing heat exchange area between solid and fluid. On the other hand, the pressure drop increases dramatically when the aspect ratio is below 1.0. Considering the balance of heat removal and pressure drop, micro-heat sink with larger microchannel and aspect ratio is expected to have a higher heat dissipation and lower-pressure drop. Owing to the fabrication capability, we chose the microchannel array with channel width of 80µm and aspect ratio of 0.8.

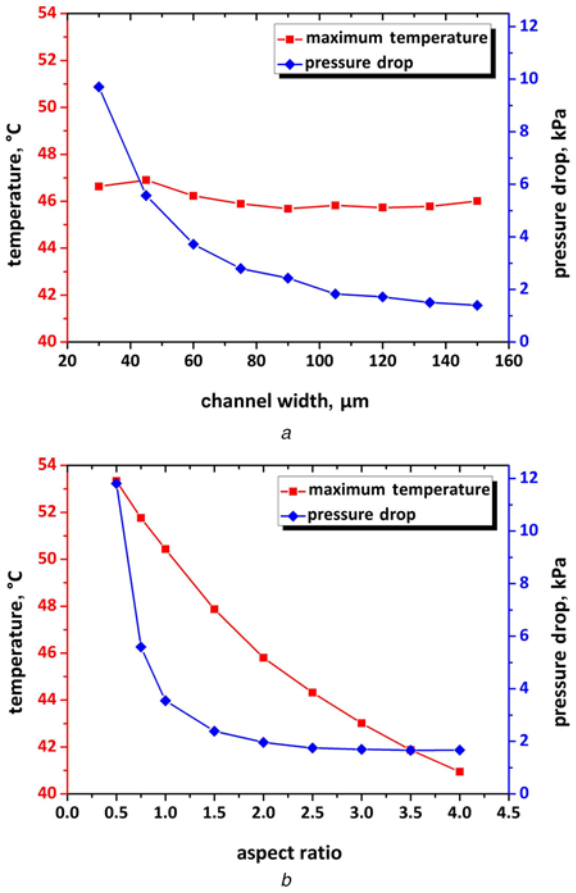

Fig. 2 *Maximum temperature and pressure drop between inlet/outlet*
a Simulation results of temperature and pressure drop of different channel width
b Simulation results of temperature and pressure drop of different aspect ratios

3. Fabrication process: The fabrication process contains tungsten die ICP etching, copper microembossing and sealing. It is shown in Fig. 3.

3.1. Tungsten die ICP etching: The tungsten dies ICP etching process provides an alternative process for microembossing die fabrication. Tungsten was cut into 5 mm thick 4 in wafers with double side polished. First, tungsten wafers were cleaned out by concentrated sulphuric acid for 24 h. Next, thin Al film was sputtered onto the front side of the tungsten wafer as hard mask. Photoresist AZ4620 was used for photolithography, and the Al thin film was patterned by dry etching (Fig. 3*a*). Next, microchannels were etched on tungsten substrate by ICP etching. To promote the aspect ratio of microchannel, a time-multiplexed process was introduced, containing etching, passivation and depassivation steps (Fig. 3*b*). Sulphur hexafluoride was used as etching gas to provide fluorine radical, whereas octafluorocyclobutane was applied in the passivation step to protect the sidewall from etching. The time-multiplexed process improves the selectivity of Al thin film (>50:1). Microchannels with large etching depth and good steepness are achieved.

The tungsten wafer was ultrasonically cleaned with acetone and isopropanol after etching to further remove grass on the bottom of microchannels. Finally, the tungsten dies were cut into the dimension of 8.0 mm × 5.0 mm × 5.0 mm by wire electrical discharge machining.

3.2. Hot copper microembossing: The hot copper microembossing is the key part of the fabrication process (Fig. 3*c*). The embossing process contains four steps: heating, embossing, cooling and

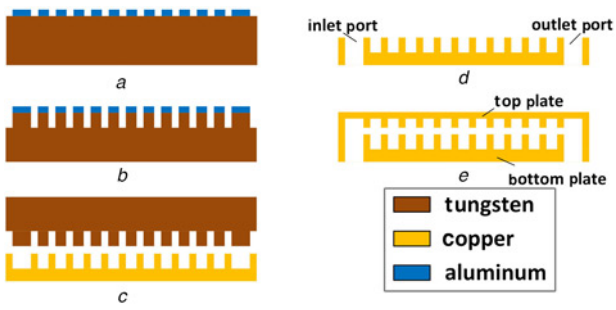

Fig. 3 *Diagram of fabrication process of copper micro-heat sink*
a Al thin-film deposition and patterning on tungsten wafer
b Tungsten dry etching
c Hot copper microembossing
d Inlet/outlet ports punching
e Top and bottom plates sealing

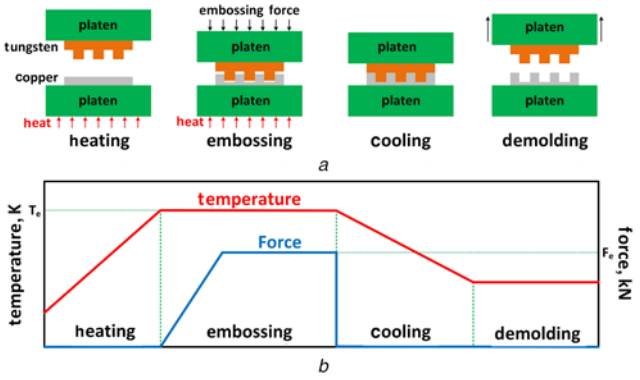

Fig. 4 *Hot copper microembossing process*
a Fabrication process of hot copper microembossing
b Corresponding temperature and force profile of microembossing

demoulding, as shown in Fig. 4*a*. The microembossing process is controlled by heating temperature and embossing force (Fig. 4*b*). The copper workpiece was first heated on the bottom plate to the setting temperature T_e. Next, the embossing force increased at a constant loading rate from 0 to F_e. Microchannel array was transferred from tungsten die to copper workpiece in this stage. Then, T_e and F_e held at a constant value. After embossing, the embossing force was first released at the cooling stage. Finally, after the workpiece cooled down to room temperature, the tungsten die and copper workpiece were separated.

The fabrication process requires a higher mechanical strength of tungsten die due to the large embossing force, and the mechanical strength of tungsten is highly related to microchannel parameters. The tungsten die fracture was observed in microchannels with higher aspect ratio and smaller microchannels. As a result, there is a contradiction between higher cooling performance and higher manufacturing success rate. In consideration of the fabrication capability and heat dissipation performance, microchannel with width of 80 µm and aspect ratio of 0.8 is applied. Microchannels are embossed on the top plate and bottom plate of the micro-heat sink.

3.3. Inlet/outlet ports punching and sealing: Inlet/outlet ports were punched onto the bottom plate after microembossing (Fig. 3*d*). Finally, the top and bottom plates were sealed by hard solder to form an enclosed micro-heat sink (Fig. 3*e*). The pressure drop between inlet/outlet ports reached at least 30 kPa without liquid leakage.

The dimensions of the micro-heat sink are shown in Table 1.

4. Experiments and results: Fig. 5 shows the microstructure of copper microchannel array. Fig. 5*a* is captured by laser confocal scanning microscope and Fig. 5*b* by scanning electron microscope (SEM). Microchannel patterns were completely transferred to the copper substrate with good surface and sidewall quality.

The micro-heat sink and the packaging box are shown in Fig. 6*a*. The packaging box is an Al box acting as the connection between micro-heat sink and inlet/outlet pipes. The ceramic heater was in circular shape with a diameter of 5 mm, and it was stuck at the top of the micro-heat sink. The schematic diagram and photograph

Table 1 Dimensions of copper micro-heat sink

Structure	Dimension
inlet/outlet diameter, mm	1.3
channel width, µm	80
channel height, µm	65
microchannel area, mm^2	5×5
heat sink size, mm^3	$10 \times 10 \times 2$

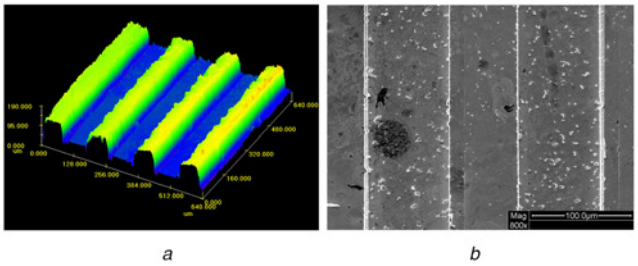

Fig. 5 *Images of microembossed channels*
a Laser confocal scanning microscope image of hot copper microembossing microchannel
b SEM image of microembossing microchannel

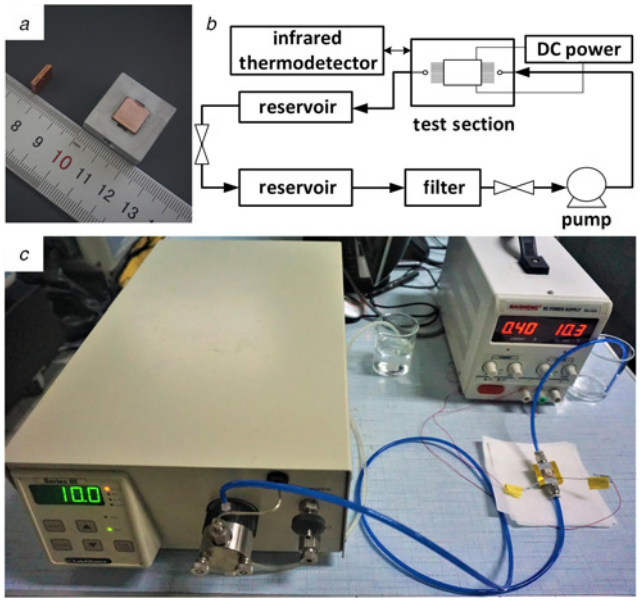

Fig. 6 *Photographs of micro-heat sink and testing module*
a Appearance of micro-heat sink and packaging box
b Schematic diagram of the testing module
c Photogram of a testing system with DC supply

of the testing system are shown in Figs. 6*b* and *c*. The heater was driven by a DC power supply to provide a uniform heat flux. Deionised water was used as coolant and a flow pump was used to provide steady flow rate. A non-contact infrared thermodetector was used to measure the temperature on the ceramic surface. In the following test, the maximum temperature, which occurs near the outlet port, was detected. The experiment was applied in the environment temperature of 25°C.

The maximum temperature on the chip surface as a function of flow rate was studied. Different heat flux was applied. The experiment result is shown in Fig. 7*a*. All the measurement errors are within ±5%. A significant drop of maximum temperature was observed as liquid flow rate increases from 0 to 30 ml/min. The maximum temperatures decrease from 95.2, 109.3, 127.1 to ~37°C at the heat fluxes of 30, 40, and 50 W/cm^2, respectively, with the maximum decreasing value for ~69.2% at 50 W/cm^2 heat flux.

The heat transfer coefficient was also used to analyse the cooling performance. The total thermal resistance contains the heat-conduction resistance of bulk copper and Al packaging box, and the heat-convection resistance between deionised water and the copper heat sink. The total thermal resistance can be written as

$$R = \frac{t_{Cu}}{k_{Cu}ab} + \frac{t_{Al}}{k_{Al}a'b'} + \frac{1}{hS} \quad (4)$$

doi: 10.1049/mnl.2019.0198

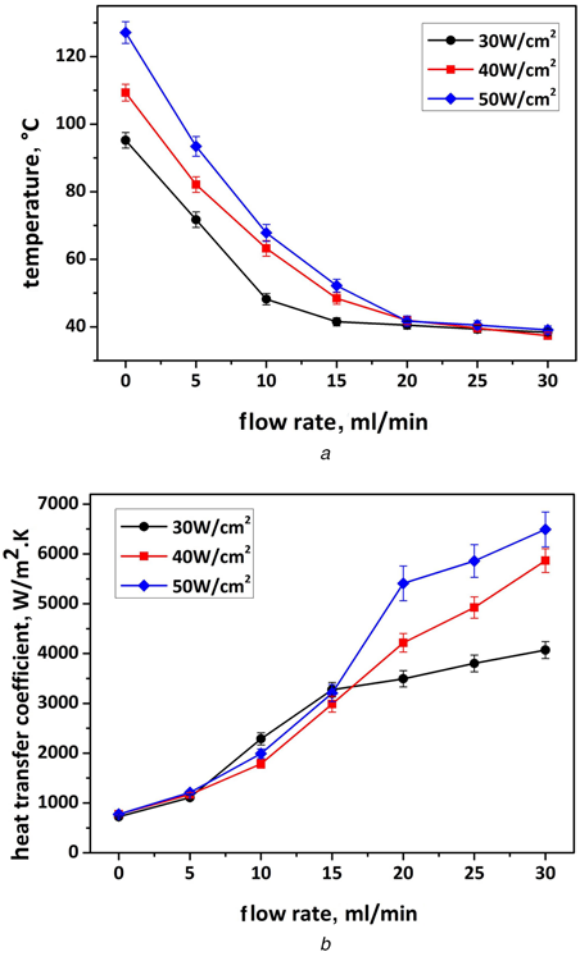

Fig. 7 *Experiment results of cooling performance of ceramic heater*
a Diagram of maximum temperature on heater surface changing with flow rate at different heat fluxes
b Heat transfer coefficient changing with flow rate at different heat fluxes

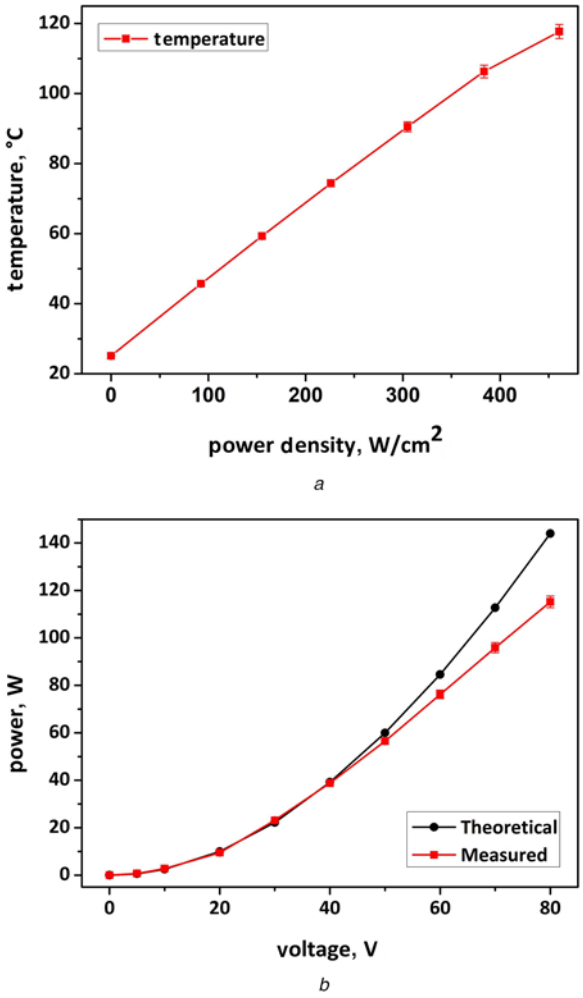

Fig. 8 *Experiment results of high-power chip applications*
a Temperature–power density curve of the high-power chip under micro-heat sink cooling
b Theoretical and measured power of the high-power chip with different voltage supplies

The first item is the heat-conduction resistance of copper, and the second item is the thermal-conduction of Al. t is the thickness of the layer and k is heat conductivity coefficient. a is the length and b is the width, and $a \times b$ represents the heat transfer area. The last item is heat-convection resistance. h is the heat transfer coefficient and S is the convection area between coolant and heat sink.

The calculated convection heat transfer coefficient is shown in Fig. 7*b*. The heat transfer coefficient increases with the increasing flow rate. For different heat fluxes, the heat transfer coefficient shows almost no difference when the flow rate is below 15 ml/min. However, when the flow rate is larger than 15 ml/min, the heat transfer coefficient increases with increasing heat flux. As shown in Fig. 7*b*, the maximum equivalent heat transfer coefficient in our experiments reaches 6492 W/m^2 K at 30 ml/min flow rate when the heat flux is 50 W/cm^2.

The cooling performance was also experimented under the high-power chip. The high-power chip was customised with an integrated heating module and a temperature sensor. It was wire bonded on a specially designed PCB board with heating port and temperature captured port. The temperature–power density curve is shown in Fig. 8*a*. The chip temperature increases from ~25 to ~100°C at 300 W/cm^2 power density, and ~120°C at 450 W/cm^2 power density. As the power density continues to increase, burning can be seen at the chip surface. The theoretical and measured values of chip power are also compared in Fig. 8*b*. The deviation between theoretical value and measurement occurs at 50 V supply and increases with voltage, which indicates that the electrical performances are affected by the high operating temperature. When the voltage is lower than 60 V, the theoretical power and the measurement show tiny differences. As the voltage continues to increase, a significant reduction is observed in the measurement result compared with theoretical value, which means that the electrical performance of high-power chip is improperly in this case. The measurement result shows that the maximum heat flux can reach 304.8 W/cm^2 when the chip can still function properly at 90.5°C.

5. Conclusions: A novel fabrication process for microchannel heat sink was raised for high-density cooling in electronics device. The microchannel width and aspect ratio were investigated. The maximum chip temperature is insensitive for microchannel width, but as the channel width decreases, the pressure drop increases significantly. Both temperature and pressure drop decrease with increasing aspect ratio. The fabrication process includes tungsten die ICP etching, hot copper microembossing, inlet/outlet port punching and top/bottom plates sealing. Considering the processing capacity and heat removal performance, we adopted microchannel array with channel width of 80 μm and aspect ratio of 0.8. The cooling test using ceramic heater shows that the maximum temperature decreased to ~37°C, with the maximum temperature decreased by 69.2% at 50 W/cm^2 heat flux. In this case, the heat transfer coefficient is 6492 W/m^2 K. In the cooling test using high-power chip, the chip temperature increases with increasing power

density. The comparison between theoretical power value and measurement show that the maximum heat flux can reach 304.8 W/cm^2 at the temperature of 90.5°C when the chip can still function properly. Good cooling performance shows that copper microembossing by tungsten die is an alternative process for microchannel heat sink fabrication with batch production and low cost, which shows promising potentials in high-density microcooling systems.

6. Acknowledgments: This project was supported by the National Natural Science Foundation of China (grant no. U1537208) and the National High Technology Research and Development Programme of China (863) grant no. 2015AA043601.

7 References

[1] Fabis P.M., Shum D., Windischmann H.: 'Thermal modeling of diamond-based power electronics packaging'. 15th Annual IEEE Semiconductor Thermal Measurement and Management Symp., San Diego, CA, USA, 1999, pp. 98–104

[2] Singh R., Akbarzadeh A., Mochizuki M., *ET AL.*: 'Thermal characterization of copper microchannel heat sink for power electronics cooling', *J. Thermophys. Heat Transf.*, 2009, **23**, (2), pp. 371–380

[3] Tuckerman D.B., Pease R.F.W.: 'High-performance heat sinking for VLSI', *IEEE Electron Device Lett.*, 1981, **2**, (5), pp. 126–129

[4] Tullius J.F., Tullius T.K., Bayazitoglu Y.: 'Optimization of short micro pin fins in minichannels', *Int. J. Heat Mass Transf.*, 2012, **55**, pp. 3921–3932

[5] Woodcock C., Yu X., Plawsky J., *ET AL.*: 'Piranha pin fin (PPF) – advanced flow boiling microstructures with low surface tension dielectric fluids', *Int. J. Heat Mass Transf.*, 2015, **90**, pp. 591–604

[6] Kewalramani G.V., Hedau G., Saha S.K., *ET AL.*: 'Study of laminar single-phase frictional factor and Nusselt number in in-line micro pin-fin heat sink for electronic cooling applications', *Int. J. Heat Mass Transf.*, 2019, **138**, pp. 796–808

[7] Lelea D.: 'Effects of inlet geometry on heat transfer and fluid flow of tangential micro-heat sink', *Int. J. Heat Mass Transf.*, 2010, **53**, pp. 3562–3569

[8] Chein R., Chen J.: 'Numerical study of the inlet/outlet arrangement effect on microchannel heat sink performance', *Int. J. Thermal Sci.*, 2009, **48**, (8), pp. 1627–1638

[9] Hung T.C., Yan W.M., Li W.P.: 'Analysis of heat transfer characteristics of double-layered microchannel heat sink', *Int. J. Heat Mass Transf.*, 2012, **55**, pp. 3090–3099

[10] Sarangi S., Bodla K.K., Garimella S.V., *ET AL.*: 'Manifold microchannel heat sink design using optimization under uncertainty', *Int. J. Heat Mass Transf.*, 2014, **69**, pp. 92–105

[11] Zhai Y., Li Z., Wang H., *ET AL.*: 'Analysis of field synergy principle and the relationship between secondary flow and heat transfer in double-layered microchannels with cavities and ribs', *Int. J. Heat Mass Transf.*, 2016, **101**, pp. 190–197

[12] Drummond K.P., Weibel J.A., Garimella S.V.: 'Experimental study of flow boiling in a compact hierarchical manifold microchannel heat sink array'. 2017 33rd Thermal Measurement, Modeling & Management Symp. (SEMI-THERM), San Jose, CA, USA, 2017, pp. 139–143

[13] Drummond K.P., Back D., Sinanis M.D., *ET AL.*: 'A hierarchical manifold microchannel heat sink array for high-heat-flux two-phase cooling of electronics', *Int. J. Heat Mass Transf.*, 2018, **117**, pp. 319–330

[14] Jang S.P., Choi S.U.S.: 'Cooling performance of a microchannel heat sink with nanofluids', *Appl. Therm. Eng.*, 2006, **26**, pp. 2457–2463

[15] Wu X., Wu H., Cheng P.: 'Pressure drop and heat transfer of Al_2O_3-H_2O nanofluids through silicon microchannels', *J. Micromech. Microeng.*, 2009, **19**, (10), p. 105020

[16] Zhao J., Wang Y., Ding G., *ET AL.*: 'Design, fabrication and measurement of a microchannel heat sink with a pin-fin array and optimal inlet position for alleviating the hot spot effect', *J. Micromech. Microeng.*, 2014, **24**, (11), p. 115013

[17] Yang D., Ding G., Wang Y., *ET AL.*: 'Heat removal capacity enhanced micropin array heat sink with optimised pin height and inlet–outlet positions', *Micro Nano Lett.*, 2016, **11**, (3), pp. 156–159

[18] Zhang H.Y., Pinjala D., Wong T.N., *ET AL.*: 'Single-phase liquid-cooled microchannel heat sink for electronic packages', *Appl. Therm. Eng.*, 2005, **25**, (10), pp. 1472–1487

[19] Jenkins R., Lupoi R., Kempers R., *ET AL.*: 'Heat transfer performance of boiling jet array impingement on micro-grooved surfaces', *Exp. Therm. Fluid Sci.*, 2017, **80**, pp. 293–304

[20] Deng D., Chen L., Chen X., *ET AL.*: 'Heat transfer and pressure drop of a periodic expanded-constrained microchannels heat sink', *Int. J. Heat Mass Transf.*, 2019, **140**, pp. 678–690

[21] Law M., Lee P.S., Balasubramanian K.: 'Experimental investigation of flow boiling heat transfer in novel oblique-finned microchannels', *Int. J. Heat Mass Transf.*, 2014, **76**, pp. 419–431

[22] Naphon P., Nakharintr L., Wiriyasart S.: 'Continuous nanofluids jet impingement heat transfer and flow in a micro-channel heat sink', *Int. J. Heat Mass Transf.*, 2018, **126**, pp. 924–932

doi: 10.1049/mnl.2019.0198